Results in Physics 58 (2024) 107507

Contents lists available at ScienceDirect

Results in Physics

journal homepage: www.elsevier.com/locate/rinp

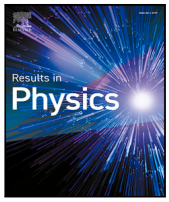

Tunable superluminal propagation at spectral hole-burning regions in magneto-optical atomic medium

Aizaz Khan [a], Xiaoying Gu [a], Lei Gao [a,b,*], Lianping Hou [c], Jehan Akbar [c,*], Dongliang Gao [a,*]

[a] School of Physical Science and Technology & Jiangsu Key Laboratory of Thin Films, Soochow University, Suzhou 215006, China
[b] School of Optical and Electronic Information, Suzhou City University & Suzhou Key Laboratory of Biophotonics, Suzhou 215104, China
[c] James Watt School of Engineering, University of Glasgow, G12 8QQ, UK

ARTICLE INFO

Keywords:
Spectral hole-burning
Density matrix formulism
Subluminal and superluminal propagation

ABSTRACT

In the context of spectral hole-burning, normal dispersion with subluminal propagation is usually observed in the spectral hole-burning depth region. However, anomalous dispersion can occur in the continuous absorption peak region, which leads to superluminal light propagation. In this paper, we report an unusual behavior of dispersion at discontinued absorption kink regions. We demonstrate both normal dispersion at the kink absorption region and anomalous dispersion at the spectral hole-burning depth region. The unusual dispersion leads to a positive group index in the absorption kink region and a negative group index in the spectral hole-burning depth region. The spectral hole-burning is due to variation of magnetization rather than the molecular distribution. The outcomes of our work offer promising applications in communication technologies and storage devices.

Introduction

The development of laser technologies has resulted in extraordinary advances in quantum optics, photonics, and plasmonics [1]. The use of coherent atomic media has enabled researchers to introduce the phenomenon of practical interests like electromagnetically induced transparency (EIT) [2], four-wave mixing [3], Kerr nonlinearity [4], electromagnetically induced absorption (EIA), and so on. Coherent control of the group index of light in an atomic medium is one of the very important phenomena. Recently, the study of light propagation in coherent media has attracted much attenion because of its potential applications in high-speed optical switching [5], photon controlling and storage [6,7], nonlinear optics [8], sensing [9,10] and quantum communication [11,12].

The group velocity of a light pulse may exceed the speed of light in a vacuum and may also slow down [13,14]. The group velocity can even be negative in transparent materials. A lot of efforts have been devoted to tune and control of the group velocity of light from one regime to the other [15]. It has been reported that at the resonance the group velocity can be tuned from subluminal to superluminal regime [16–18]. More interestingly, a balance between linear and non-linear effects in coherent media resulting in optical soliton with a negative group index has been reported [19,20]. Sahrai et al. [21,22] studied tunable control of the group velocity of a weak probe pulse varying from ultra-slow to ultra-fast propagation through the variation of the relative phase and intensity of the driving field. The enhanced effects of ultra-fast and ultra-low propagation have been experimentally demonstrated based on EIT and EIA [23]. The tunability of the group index of light is studied extensively in various media such as atomic media [24], semi-metals [25] and photonic-crystals [26].

Spectral hole-burning (SHB) [27,28] is a phenomenon wherein a saturating field induces a hole within the population distribution of an inhomogeneous medium. This phenomenon has widespread applications in the realms of atomic, molecular, and solid-state physics [29,30]. It offers promising prospects for the development of robust devices for functions such as data storage (in the form of optical memory) and signal processing [31,32]. Additionally, SHB finds utility in frequency stabilization [33], optical tomography [34] and spectral-spatial correlation studies [35]. Dong and Gao reported the observation of coherent SHB within a Doppler broadening medium by employing coupling and saturating laser beams [36]. In contrast, a comparative analysis of coherent holes in various atomic mediums shows that SHB exhibits dominance within the Λ-type atomic configuration [37].

The tunability of light propagation from one to the other regime is still a topic of concern. Over recent years, numerous works have been focused on achieving tunable control of group velocity using various techniques and methodologies. The tunable control of group velocity within the SHB regions is remarkably a largely unexplored domain within the field of the high magneto-optical atomic medium [38,39].

* Corresponding authors.
E-mail addresses: leigao@suda.edu.cn (L. Gao), jehan.akbar@glasgow.ac.uk (J. Akbar), dlgao@suda.edu.cn (D. Gao).

https://doi.org/10.1016/j.rinp.2024.107507
Received 26 October 2023; Received in revised form 9 February 2024; Accepted 20 February 2024
Available online 21 February 2024
2211-3797/© 2024 The Author(s). Published by Elsevier B.V. This is an open access article under the CC BY-NC-ND license (http://creativecommons.org/licenses/by-nc-nd/4.0/).

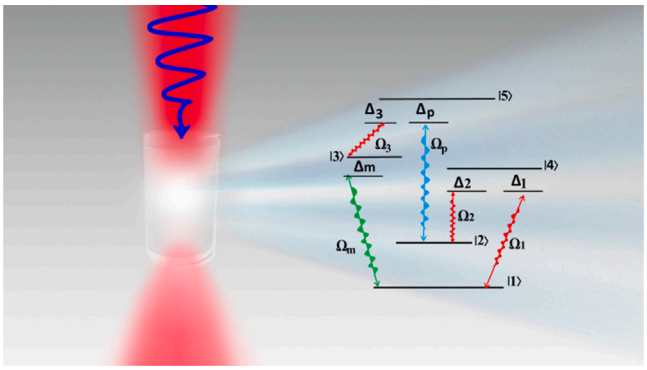

Fig. 1. Schematics of a five-level high magneto-optical atomic medium driving by coherent electromagnetic probe and control fields, as visualized in 3D. Five-level scheme showing various couplings. The two ground states are taken in superposition. The electric and magnetic components couple the transitions |2⟩-|5⟩ and |1⟩-|3⟩, respectively.

The primary motivation driving this paper is the exploration of transitions between different modes of light propagation at SHB regions which is a matter of considerable significance within the research community. We have achieved the group velocity's modulation through precise control of system parameters such as phase, Rabi frequencies, and detuning. Our research unveils the presence of both single and double SHB regions, wherein both normal and anomalous dispersions have been investigated. The group index and delay time are also studied to support our results. An observation of particular significance is the unusual behavior of dispersion within these regions. Moreover, normal dispersion occurs at the kink absorption region, while anomalous dispersion manifests the SHB depth region. Furthermore, it is important to emphasize that this SHB phenomenon is not attributed to the molecular distribution but rather it is due to the variations in magnetization. Consequently, the five-level high magneto-optical atomic medium might offer advantages over other atomic media. The significance of this study goes beyond pure scientific inquiry as it carries the potential for a wide range of applications in the fields of communication technology and storage devices.

Model of the atomic system

As shown in Fig. 1, a high magneto-optical medium composed of five-level atoms is considered for the tunable control of subluminal to superluminal propagation of probe beams at the SHB regions. An electric probe field denoted as E_p, characterized by its Rabi frequency Ω_p and detuning Δ_p, is employed to couple the states $|2\rangle$ and $|5\rangle$. Simultaneously, a magnetic probe field denoted as B_p with its Rabi frequency Ω_m and detuning Δ_m, is applied to induce transitions between states $|1\rangle$ and $|3\rangle$. Control field E_i having Rabi frequency Ω_i and detuning Δ_i is driving between different levels as shown in Fig. 1. By employing the dipole and rotatory wave approximations, we derive the Hamiltonian for the proposed high-magneto-optical medium in the interaction picture.

$$\begin{aligned} H_I = -\frac{\hbar}{2}[&\Omega_m e^{-i\Delta_m t}|1\rangle\langle 3| + \Omega_p e^{-i\Delta_p t}|2\rangle\langle 5| + \\ &\Omega_1 e^{-i\Delta_1 t}|1\rangle\langle 4| + \Omega_2 e^{-i\Delta_2 t}|2\rangle\langle 4| + \\ &\Omega_3 e^{-i\Delta_3 t}|3\rangle\langle 5|] + H.c. \end{aligned} \tag{1}$$

The atomic states resonance frequencies ω_{ij} are related to the detunings of the probe and control fields by $\Delta_i = \omega_{ij} - \omega_i$, where ω_i is the angular frequency of the driving field. Moreover, H.c is the hermitian conjugate of each term. The dynamics of the proposed atomic system is studied using the general master equation in terms of the interaction Hamiltonian as [40–42]:

$$\dot{\rho} = -\frac{i}{\hbar}[\rho, H_I] - \frac{1}{2}\sum \gamma_{ji}(\varsigma^{\dagger}\varsigma\rho + \rho\varsigma^{\dagger}\varsigma - 2\varsigma\rho\varsigma^{\dagger}). \tag{2}$$

Where ρ is the density operator, $\varsigma^{\dagger}$ is the raising operator, ς is the lowering operator, and γ_{ji} is the decay rate. By putting the interaction Hamiltonian in Eq. (2), taking the summation over all the decays γ_{ji} and using $\rho = \widetilde{\rho}_{ij}e^{-i\Delta_i t}$, we obtained the following coupled rate equations which describe the dynamics of the proposed system.

$$\begin{aligned}
\dot{\widetilde{\rho}}_{13} &= A_1\widetilde{\rho}_{13} + \frac{i}{2}[\Omega_m(\widetilde{\rho}_{33} - \widetilde{\rho}_{11}) + \Omega_1\widetilde{\rho}_{43} - \Omega_1^*\widetilde{\rho}_{15}],\\
\dot{\widetilde{\rho}}_{15} &= A_2\widetilde{\rho}_{15} + \frac{i}{2}[\Omega_m\widetilde{\rho}_{35} + \Omega_1\widetilde{\rho}_{45} - \Omega_p\widetilde{\rho}_{12} - \Omega_3\widetilde{\rho}_{13}],\\
\dot{\widetilde{\rho}}_{45} &= A_3\widetilde{\rho}_{45} + \frac{i}{2}[\Omega_1^*\widetilde{\rho}_{15} + \Omega_2^*\widetilde{\rho}_{25} - \Omega_p\widetilde{\rho}_{42} - \Omega_3\widetilde{\rho}_{43}],\\
\dot{\widetilde{\rho}}_{25} &= A_4\widetilde{\rho}_{25} + \frac{i}{2}[\Omega_p(\widetilde{\rho}_{55} - \widetilde{\rho}_{22}) + \Omega_2^*\widetilde{\rho}_{45} - \Omega_3\widetilde{\rho}_{23}],\\
\dot{\widetilde{\rho}}_{23} &= A_5\widetilde{\rho}_{23} + \frac{i}{2}[\Omega_p\widetilde{\rho}_{53} + \Omega_2\widetilde{\rho}_{43} - \Omega_m\widetilde{\rho}_{21} - \Omega_3^*\widetilde{\rho}_{25}],\\
\dot{\widetilde{\rho}}_{43} &= A_6\widetilde{\rho}_{43} + \frac{i}{2}[\Omega_1^*\widetilde{\rho}_{13} + \Omega_2^*\widetilde{\rho}_{23} - \Omega_m\widetilde{\rho}_{41} - \Omega_3^*\widetilde{\rho}_{25}],
\end{aligned}$$

where A_i is given in the appendix. Initially, the atoms are prepared in the ground states $|1\rangle$ and $|2\rangle$. Therefore, we consider their superposition as, $|\Psi\rangle = a|1\rangle + b|2\rangle$. The co-efficients are given as $a = \sqrt{x}$ and $b = e^{i\phi}\sqrt{1-x}$. We construct the zeroth order density matrix using the definition $\widetilde{\rho}^{(0)} = |\Psi\rangle\langle\Psi|$ and obtained the matrix elements i.e., $\widetilde{\rho}_{11}^{(0)} = x$, $\widetilde{\rho}_{12}^{(0)} = e^{-i\phi}\sqrt{x(1-x)}$, $\widetilde{\rho}_{21}^{(0)} = e^{i\phi}\sqrt{x(1-x)}$, $\widetilde{\rho}_{22}^{(0)} = 1-x$ and all other matrix elements are zero. To obtain the coherences, the above rate equations have been solved by the integral $\mathcal{L}(t) = \int_{-\infty}^{t} e^{-\mathcal{G}(t-t')}\mathcal{Q}dt' = \mathcal{G}^{-1}\mathcal{Q}$. Here, both $\mathcal{L}(t)$ and $\mathcal{Q}$ are represented as column matrices, and $\mathcal{G}$ is a square matrix. After simplification, we get the electric and magnetic probe field coherences i.e. $\widetilde{\rho}_{25}^{(1)}$ and $\widetilde{\rho}_{13}^{(1)}$ respectively.

$$\widetilde{\rho}_{25}^{(1)} = \frac{B_1\Omega_m + B_2\Omega_p}{B_3}, \tag{3}$$

$$\widetilde{\rho}_{13}^{(1)} = \frac{B_4\Omega_m + B_5\Omega_p}{B_6}. \tag{4}$$

The parameters B_i are given in the appendix. To determine the electric susceptibility, we express the polarization of the medium as $P = \epsilon_0\chi_e E$. Additionally, considering the coherence of the electric probe field, the polarization takes the form $P = N|\sigma_{25}|\widetilde{\rho}_{25}^{(1)}$, where σ_{25} represents the electric dipole matrix element, defined as $\sigma_{25} = (3\hbar\epsilon_0\gamma_{52}\lambda^3/8\pi^2)^{1/2}$, and N denotes the atomic density. By comparing these relationships, we derive the complex electric susceptibility of the medium, which is presented below.

$$\chi_e = \frac{2N\sigma_{25}(B_1\mu_{13} + cB_2\sigma_{25})}{\epsilon_0\hbar cB_3}. \tag{5}$$

The atomic medium is also driven by a magnetic weak probe field. The magnetization caused due to this weak probe field in terms of magnetic dipole moment i.e. $\mu_{13} = c(3\hbar\epsilon_0\gamma_{31}\lambda^3/8\pi^2)^{1/2}$ and magnetic coherence $\widetilde{\rho}_{13}^{(1)}$ is given by $M = N\mu_{13}\rho_{13}^{(1)}$. Similarly, the induced magnetization is related to magnetic susceptibility χ_m by the relation $\chi_m = M/H$. Using $B_p = \mu_0(M + H)$ along with $B_p = E_p/c$, we obtained the magnetic susceptibility as:

$$\chi_m = -1 + \frac{B_6\hbar}{B_6\hbar - N\mu_{13}(B_4\mu_{13} + cB_5\sigma_{25})\mu_0}. \tag{6}$$

We calculated the permittivity of the medium from electrical susceptibility as $\epsilon_r = 1 + \chi_e$. Similarly, from magnetic susceptibility the relative permeability of the medium is obtained as $\mu_r = 1 + \chi_m$. Given that the refractive index of a high-magneto optical medium is a complex function that can be calculated by using $n_r = \sqrt{\epsilon_r\mu_r}$. For a five-level atomic medium, it takes the following form.

$$n_r = \left(\frac{B_6(1+\mathcal{R})\hbar}{B_6\hbar - N\mu_{13}(B_4\mu_{13} + cB_5\sigma_{25})\mu_0}\right)^{1/2}, \tag{7}$$

where $\mathcal{R}$ is written as:

$$\mathcal{R} = \frac{2N\sigma_{25}(B_1\mu_{13} + cB_2\sigma_{25})}{c\epsilon_0\hbar B_3}. \tag{8}$$

The wave-vector k is dependent upon the refractive index as $k = k_0 n_r$. The wave-vector of the propagating weak probe fields therefore becomes $k = k_0\sqrt{\epsilon_r \mu_r}$. The equation that governs the relation between group index n_g and refractive index n_r of the system is given below.

$$n_g = n_r + \omega \frac{\partial n_r}{\partial \omega}, \tag{9}$$

where $\partial n_r/\partial\omega$ is the slope representing the dispersions. The delay time t_g is the difference of time in the medium t_m to the time in vacuum t_v at the same length L that is written as $t_g = t_m - t_v$, where $t_v = L/c$ and $t_m = L/v_g$ and $v_g = c/n_g$. Plugging these values in delay time, we get $t_g = L(n_g - 1)/c$. This relation shows that the delay is positive if $n_g > 1$. Under this condition, $t_m > t_v$, and hence the speed of light in a medium is lower than the speed of light in a vacuum. If $n_g < 1$ or t_g is negative then $t_m < t_v$, then the speed of light in the medium is faster than that of vacuum.

Results and discussion

We have traced plots representing the real and imaginary components of the wave vector, denoted as k, which have been normalized to the reference wave vector k_0. The results for the group index and delay time are also simulated as functions of the normalized probe field detuning, Δ_p/γ. The imaginary part of the wave vector, denoted as Im(k), governs the absorption spectrum of the weak probe field. On the other hand, the real part of the wave vector, Re(k), is associated with the dispersion spectrum of the probe field, which describes how the phase velocity of the wave changes with frequency. Generally, superluminal propagation is reported at probe field frequencies at which high absorption occurs, and subluminal propagation in regions characterized by SHB (Low absorption) as evident from literature [43]. In this paper, we report two distinct SHB regions, there is superluminal propagation of light in one of these regions while subluminal propagation in the other region. More importantly, we report a distinctive phenomenon that we have referred to as "kink-type SHB" in the region where there is a discontinuity at the absorption peak. In this region, the absorption of light exhibits unusual behavior i.e., the results show alternating subluminal and superluminal propagation of light pulses in the kink and SHB regions. To obtain our results, we assumed an atomic decay rate of 1 GHz and scaled all other frequency-related parameters accordingly, relative to this decay rate γ. Additional parameters utilized in simulation include the magnetic decay rate, γ_{31} which is taken as $(2/137)\gamma$, angular frequency ω set to $10^4\gamma$ [21] and wavelength λ is calculated as $2\pi c/\omega$.

In Fig. 2, the absorption ($Im(k)$) is plotted as a function of the normalized probe field detuning, Δ_p/γ. The imaginary part of the wave vector is normalized by the reference wave vector k_0. The SHB is the selective frequency bleaching within the absorption spectrum [44,45].

Our analysis focuses on two distinct types of SHB theoretically associated with the absorption spectrum i.e., the holes that appear after the "discontinuous absorption kink" and the "continuous absorption hole". Our primary objective is to identify the presence of these SHBs in the absorption spectrum and subsequently categorize them as either "discontinuous kinks" or "continuous absorption holes". We examined the dispersion behavior of these two types of SHB in the subsequent plots presented in Fig. 3. The absorption is studied at various strengths of the control field. When the Rabi frequency $|\Omega_3| = 3\gamma$, the absorption spectrum exhibits two depths, precisely at probe field detunings of $\Delta_p = -2\gamma$ and $\Delta_p = 1\gamma$. The values of parameters are adjusted to $\Delta_1 = 0.9\gamma$, $\Delta_2 = -0.8\gamma$, $\Delta_3 = -0.6\gamma$, $|\Omega_{1,2}| = 3\gamma$, $\varphi = \pi$, $\varphi_1 = \pi/12$, $\varphi_2 = \pi/2$, and $\varphi_3 = \pi/15$. Notably, the SHB at $\Delta_p = -2\gamma$ occurs after a discontinuous absorption kink region, while the other SHB at $\Delta_p = 1\gamma$ is reported after a continuous absorption region. The presence of these kinks and sharp peaks is clearly illustrated in Fig. 2a. Under an alternative set of parameters, $\Delta_1 = -0.6\gamma$, $\Delta_3 = -0.6\gamma$, $|\Omega_{1,2,3}| = 0.3\gamma$,

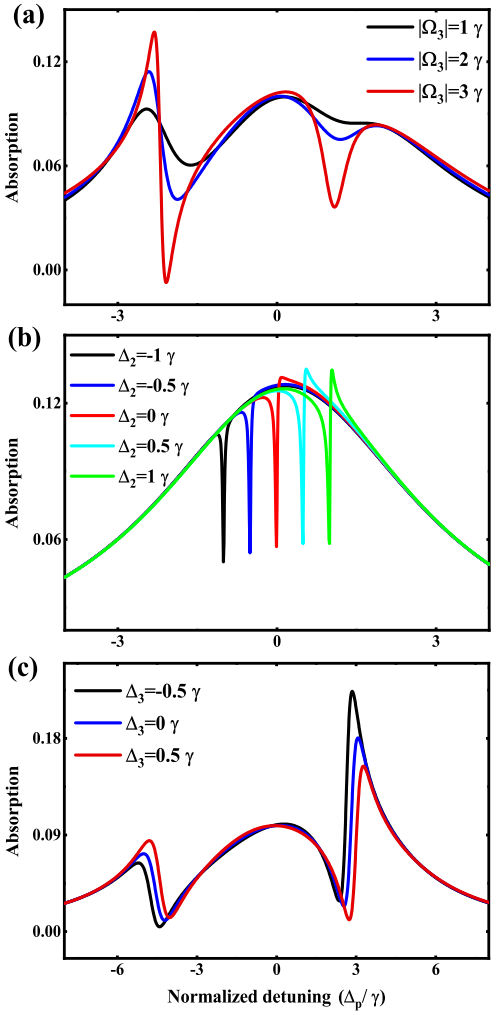

Fig. 2. The absorption is plotted against the normalized probe field detuning Δ_p/γ. (a) A spectral hole-burning after discontinuous kink at $\Delta_p/\gamma = -2$ and 1, respectively. (b) Spectral hole-burning in continuous absorption spectrum at $\Delta_p/\gamma = -1, -0.5, 0, 0.5, 1$. (c) Spectral hole-burning after kinks in the absorption at $\Delta_p/\gamma = -5, 3$.

$\phi = -\pi/6$, $\phi_1 = -\pi/2$, $\phi_2 = -\pi/6$, and $\phi_3 = -\pi/4$, a single SHB is reported within a continuous absorption spectrum. Without changing the peak value of absorption, the frequency at which this SHB appears depends upon the relative value of the detuning Δ_2, as can be seen in Fig. 2b. Tuning the controlling parameters to $\Delta_1 = -0.1\gamma$, $\Delta_2 = -0.9\gamma$, $|\Omega_{2,3}| = 4\gamma$, $\phi = 0$, $\phi_1 = 0$, $\phi_2 = -\pi/8$, and $\phi_3 = -\pi/7$, the occurrence of kinks in the absorption spectrum are reported, accompanied by SHBs. These SHB after kinks manifest at probe field detunings of $\Delta_p = -5\gamma$ and $\Delta_p = 3\gamma$ as shown in Fig. 2c. In this case, the peak of absorptions shows an alternate behavior with Δ_3, it can be seen that as the peak value of one kink reduces, the peak value of other kink regions starts to enhance with Δ_3.

In Fig. 3, we have plotted the real component of the normalized wave vector k/k_0, against the normalized probe field detuning. Normal dispersion is associated with a positive group index and hence slow light propagation.

Conversely, anomalous dispersion corresponds to ultra-fast propagation (superluminality) and is characterized by a negative group index. We studied the dispersion profiles of both types of SHBs, namely the "discontinuous kink" and "continuous absorption spectral-hole". We maintain the same parameters as used in Fig. 2, for which the corresponding SHB in the absorption spectrum were observed. When using the same parameters as Fig. 2a, alternate normal and anomalous

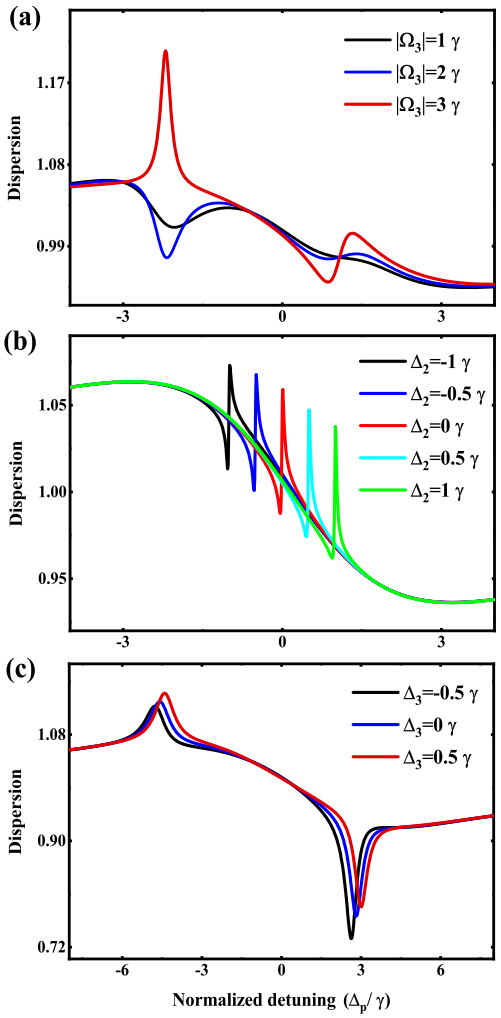

Fig. 3. The dispersion $Re(k/k_0)$ is plotted against the probe field detuning Δ_p/γ. (a) Normal and anomalous dispersion can be observed at the discontinuous kink and spectral hole-burning, respectively. It can be seen that the dispersion profile for the values of Δ_p/γ between −3 and −1 is totally opposite from the other two results. (b) Usual steep and normal dispersion at the spectral hole-burning. (c) Dispersion profile of kinks at both the negative and positive frequencies.

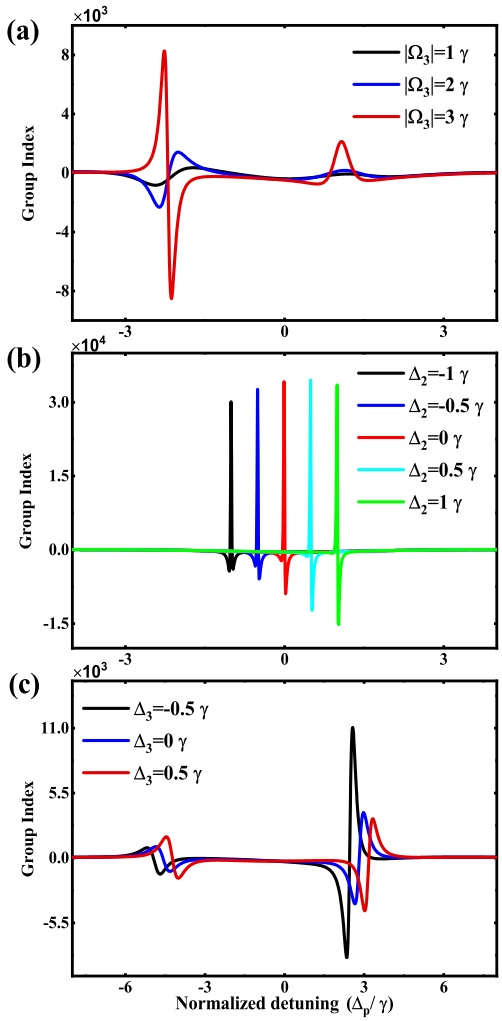

Fig. 4. Group index is plotted vs. Δ_p/γ, using the same parameters as Fig. 2. (a) Positive group index at the kink frequency and negative group index at the spectral hole-burning region, while the group index is positive at the continuous absorption frequency. (b) Positive group index at the continuous spectral hole-burning frequency. (c) Conversely, positive group index in the kink frequency and negative group index in the spectral hole-burning region.

dispersions are reported, specifically, when $|\ \Omega_3\ | = 3\gamma$. It is noteworthy that these dispersive behaviors align with the absorption kink and SHB regions, respectively. This observation deviates from the typical behavior. However, in the region of the second SHB, which is reported after continuous absorption, we observe anomalous and normal dispersions at the continuous absorption peak region and SHB depth region, respectively, as depicted in Fig. 3a. In a scenario using the same parameters as similar to Fig. 2b, where SHB occurs within continuous absorption, the dispersion slope is steep and normal, as demonstrated in Fig. 3b. Under the same parameters as Fig. 2c, where we observed alternating kinks in absorption and SHB at $\Delta_p = -5\gamma$ and $\Delta_p = 3\gamma$, the unusual dispersion for both negative and positive frequencies are reported, as illustrated in Fig. 3c.

To validate the above results it is important to look for the behavior of the group index and delay/advance time at those frequencies where such SHB is reported. Therefore, in Fig. 4, we plot the group index, denoted as n_g, as a function of the normalized probe field detuning. It is important to note that the behavior of the group index is tied to the dispersion properties of the medium. Specifically, during steep normal dispersion, the group index assumes a positive value, and this value is notably enhanced. In contrast, in the region of anomalous dispersion, the group index attains a large but negative value. In the SHB region, specifically at $\Delta_p = -2\gamma$ as depicted in Fig. 2a, we investigate a rather unconventional dispersion behavior.

In the absorption kink region, the group index exhibits a highly positive value, while in the SHB depth region, it takes on a significant negative value. However, in the continuous absorption region normal dispersion leads to an enhancement of the positive group index, as demonstrated in Fig. 4a. Under the same parameters as in Fig. 2b, where a single SHB takes place at various values of Δ_p within a continuous spectrum, the group index experiences a significant boost, but positive. This increase in the group index leads to a reduction in the group velocity, as illustrated in Fig. 4b. With parameters matching those of Fig. 2c, where unusual dispersion arises due to the discontinuous absorption kink and SHB depth region, the group index is alternately positive and negative at negative detuning, and its value changes from negative to positive at positive probe field detuning. But the same behavior as Fig. 4a seems to be valid in this case as shown in Fig. 4c.

In Fig. 5, the results are traced for delay time as a function of the normalized probe field detuning, represented as Δ_p/γ. It is important to note that the behavior of delay time is closely associated with the group

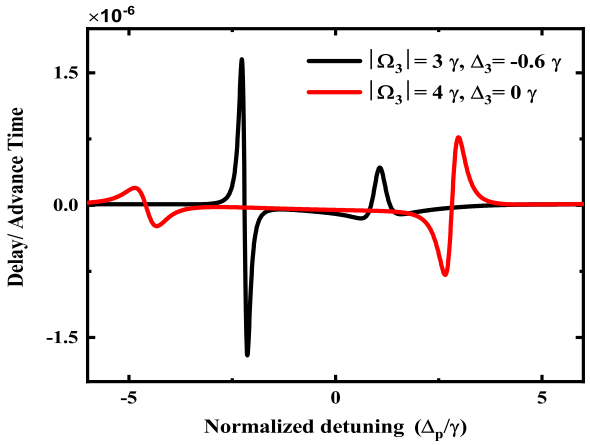

Fig. 5. Delay time t_g have been plotted against the normalized probe field detuning Δ_p/γ for medium of length $L = 0.06$ m. Considering the black curve, t_g is positive at the kink frequency and negative at the spectral hole-burning region, similarly t_g is positive at the continuous spectral hole-burning region. The t_g is positive at the kink frequency and negative at the spectral hole-burning region at both negative and positive probe detuning as evident from red curve. (For interpretation of the references to color in this figure legend, the reader is referred to the web version of this article.)

index. Specifically, when the group index is negative, the group velocity v_g also becomes negative. In this situation, t_m is less than t_v, indicating negative group velocity which leads to superluminal propagation. By utilizing the same parameters as those in Fig. 2a, which corresponds to the region of unusual dispersion associated with SHB, we report a delay time of approximately ±1.5 μs. In contrast for the typical dispersion region, the delay time is 0.5 μs, which is significantly shorter as illustrated in Fig. 5 (black curve). Using the same parameters as Fig. 2c, which pertain to the unusual dispersion behavior observed in the regions of absorption kink and SHB depth at $\Delta_p = -5\gamma$ and $\Delta_p = 2.5\gamma$, the t_g are approximately ±0.3 μs and ±1 μs, respectively, as presented in Fig. 5 (red curve).

Conclusions

In this paper, the spectral hole-burning and related subluminal/superluminal propagation of probe are controlled and modified in a high magneto-optical medium. The density matrix approach is used as the underlying theory for the calculations of the refractive index of the high magneto-optical medium. The unusual behavior of dispersion is investigated at the discontinued absorption kink region. At the kink absorption region, normal and spectral hole-burning depth region anomalous dispersion is observed, which shows a contrasting behavior in the case when spectral hole-burning occurs in a continuous absorption region. Due to unusual dispersion positive group index in the absorption kink region and a negative group index in the spectral hole-burning depth region are reported. It is important to note that the spectral hole-burning is reported due to magnetization variation, which offers an advantage of this medium over the other schemes of spectral hole-burning. The results reported in this manuscript have potential applications in communication technology and storage devices.

CRediT authorship contribution statement

Aizaz Khan: Writing – review & editing, Writing – original draft, Software, Methodology, Conceptualization. **Xiaoying Gu:** Writing – review & editing, Visualization. **Lei Gao:** Writing – review & editing, Supervision, Conceptualization. **Lianping Hou:** Validation, Formal analysis. **Jehan Akbar:** Writing – review & editing, Supervision, Conceptualization. **Dongliang Gao:** Writing – review & editing, Supervision, Funding acquisition, Conceptualization.

Declaration of competing interest

The authors declare that they have no known competing financial interests or personal relationships that could have appeared to influence the work reported in this paper.

Data availability

Data will be made available on request.

Acknowledgment

This work was supported by the National Natural Science Foundation of China (12174281, 12274314); Natural Science Foundation of Jiangsu Province, China (BK20221240); Suzhou Basic Research Project (SJC2023003); Collaborative Innovation Center of Suzhou Nano Science and Technology.

Appendix

The parameters A_i and B_i for the coupled rate equations and coherences are given by the following expressions.

$$A_1 = i\Delta_m - \frac{1}{2}(\gamma_{41}+\gamma_{31}+\gamma_{53}),$$
$$A_2 = i(\Delta_3+\Delta_m) - \frac{1}{2}(\gamma_{31}+\gamma_{41}),$$
$$A_3 = i(\Delta_m+\Delta_3-\Delta_1),$$
$$A_4 = i\Delta_p - \frac{1}{2}(\gamma_{42}+\gamma_{52}),$$
$$A_5 = i(\Delta_p-\Delta_3) - \frac{1}{2}(\gamma_{42}+\gamma_{52}+\gamma_{53}),$$
$$A_6 = i(\Delta_m-\Delta_1) - \frac{1}{2}\gamma_{53},$$
$$A_7 = \frac{i\exp(\imath\phi\sqrt{x(1-x)})}{2},$$
$$A_8 = i(1-x)$$
$$A_9 = \frac{i\exp(-\imath\phi\sqrt{x(1-x)})}{2},$$

$$\begin{aligned}B_1 = {} & -2i(A_9|\Omega_1|^4|\Omega_3| + A_9|\Omega_2|^2|\Omega_3|\varrho_2 + A_9\\ & |\Omega_3|\varrho_2\varrho_4)e^{i\phi_3} - |\Omega_1|^3|\Omega_2||\Omega_3|xe^{i(\phi_3+\phi_2-\phi_1)}\\ & + 4e^{i(\phi_3-\phi_1)}|\Omega_1||\Omega_3|\varrho_{14} + |\Omega_3|^2\varrho_{16} + |\Omega_2|^2\varrho_{15},\end{aligned}$$
$$\begin{aligned}B_2 = {} & -4A_5A_8|\Omega_1|^4 + 4A_5A_7e^{i(\phi_2-\phi_1)}|\Omega_1|^3|\Omega_2|\\ & - 4A_3A_8|\Omega_2|^2\varrho_2 - 4A_5A_8\varrho_2\varrho_4 - e^{-i\phi}|\Omega_1|\\ & (|\Omega_2|^2\varrho_{13} + 16A_5(A_2A_3A_8e^{i\phi_1}|\Omega_1| - A_1A_6\\ & \varrho_{10}) + 4\varrho_{12}|\Omega_3|^2),\end{aligned}$$

$$\begin{aligned}B_3 = {} & (|\Omega_1|^2\varrho_1 + \varrho_2(4\varrho_3|\Omega_2|^2 + |\Omega_2|^4 + \varrho_4\varrho_1)\\ & + 2|\Omega_1|^2(2\varrho_5|\Omega_2|^2 + \varrho_1\varrho_6)),\end{aligned}$$

$$\begin{aligned}B_4 = {} & 2i\varrho_9A_9e^{i\phi_1}|\Omega_1||\Omega_3|^2 - 2iA_6|\Omega_1|\varrho_1x - 2iA_2\\ & \varrho_4\varrho_1x - 2ie^{-i\phi_2}(A_4|\Omega_1|^2|\Omega_2|\varrho_7 - A_2|\Omega_2|^3\varrho_7\\ & - 4A_2|\Omega_2|\varrho_8).\end{aligned}$$
$$\begin{aligned}B_5 = {} & -8i(\varrho_{11}A_8e^{i\phi_1}|\Omega_1| - \varrho_3A_7e^{i\phi_2}R_2) - 2ie^{-i\phi_3}\\ & |\Omega_1|^2\varrho_{10}|\Omega_3| - 2ie^{-i(\phi_2+\phi_3)}|\Omega_2|^3\varrho_{10}|\Omega_3|\\ & - A_8e^{i\phi_1}|\Omega_1||\Omega_3|^2 +\\ & 2iA_7e^{-i\phi_3}|\Omega_1|^2|\Omega_3|\varrho_1 - 2iA_7e^{-i\phi_3}|\Omega_3|\varrho_4\varrho_2,\end{aligned}$$
$$\begin{aligned}B_6 = {} & (|\Omega_1|^4\varrho_1 + \varrho_2(4\varrho_3|\Omega_2|^2 + |\Omega_2|^4 + \varrho_4\varrho_1)\\ & + 2|\Omega_1|^2(2\varrho_5|\Omega_2|^2 + \varrho_1\varrho_6)).\end{aligned}$$

Where ϱ_i is given by the following relations

$$\varrho_1 = 4A_4A_5 + |\Omega_3|^2,$$

$$
\begin{aligned}
\varrho_2 &= 4A_1A_2 - |\Omega_3|^2,\\
\varrho_3 &= A_3A_4 + A_5A_6,\\
\varrho_4 &= 4A_3A_6 - |\Omega_3|^2,\\
\varrho_5 &= A_1A_4 + A_2A_5,\\
\varrho_6 &= 2A_2A_3 + 2A_1A_6 + |\Omega_3|^2,\\
\varrho_7 &= 2iA_9e^{i\phi_1}|\Omega_1| + e^{i\phi_2}|\Omega_2|x,\\
\varrho_8 &= 2iA_3A_4A_9e^{i\phi_1}|\Omega_1| + (A_3A_4|\Omega_2|x + A_5A_6\\
&\quad |\Omega_2|x)e^{i\phi_2},\\
\varrho_9 &= A_2 - A_4 + A_6,\\
\varrho_{10} &= -A_8e^{i\phi_1}|\Omega_1| + A_7e^{i\phi_2}|\Omega_2|,\\
\varrho_{11} &= A_2(A_3 + A_5) + A_5A_6,
\end{aligned}
$$

$$
\begin{aligned}
\varrho_{12} &= 2A_5A_8|\Omega_1|e^{i\phi_1} + (A_1 + A_3 - A_5)A_7|\Omega_2|e^{i\phi_2},\\
\varrho_{13} &= 4A_1A_8|\Omega_1|e^{i\phi_1} + 4A_1A_7|\Omega_2|e^{i\phi_2},\\
\varrho_{14} &= -2i(a_2A_3 + A_1A_6)A_9|\Omega_1|e^{i\phi_1} + (A_2(A_5 - A_3)\\
&\quad + A_5A_6)|\Omega_2|xe^{i\phi_2},\\
\varrho_{15} &= 2iA_9|\Omega_1||\Omega_3|e^{i(\phi_1+\phi_3)} + |\Omega_2||\Omega_3|xe^{i(\phi_2+\phi_3)},\\
\varrho_{16} &= -4iA_9|\Omega_1||\Omega_3|e^{i(\phi_1+\phi_3)} - |\Omega_2||\Omega_3|xe^{i(\phi_2+\phi_3)}.
\end{aligned}
$$

References

[1] Yu H, Peng Y, Yang Y, Li ZY. Plasmon-enhanced light–matter interactions and applications. NPJ Comput Mater 2019;5:45. http://dx.doi.org/10.1038/s41524-019-0184-1.

[2] Fleischhauer M, Imamoglu A, Marangos JP. Electromagnetically induced transparency: Optics in coherent media. Rev Modern Phys 2005;77:633. http://dx.doi.org/10.1103/RevModPhys.77.633.

[3] Deng L, Hagley EW, Wen J, Trippenbach M, Band Y, Julienne PS, Phillips WD. Four-wave mixing with matter waves. Nature 1999;398:218. http://dx.doi.org/10.1038/18395.

[4] Wang H, Goorskey D, Xiao M. Enhanced Kerr nonlinearity via atomic coherence in a three-level atomic system. Phys Rev Lett 2001;87:073601. http://dx.doi.org/10.1103/PhysRevLett.87.073601.

[5] Bajcsy M, Hofferberth S, Balic V, Peyronel T, Hafezi M, Zibrov AS, Lukin MD. Efficient all-optical switching using slow light within a hollow fiber. Phys Rev Lett 2009;102:203902. http://dx.doi.org/10.1103/PhysRevLett.102.203902.

[6] Liu C, Dutton Z, Behroozi CH, Hau LV. Observation of coherent optical information storage in an atomic medium using halted light pulses. Nature 2001;409:490. http://dx.doi.org/10.1038/35054017.

[7] Chen Z, Segev M. Highlighting photonics: looking into the next decade. eLight 2021;1:2. http://dx.doi.org/10.1186/s43593-021-00002-y.

[8] Hou J, Situ G. Image encryption using spatial nonlinear optics. eLight 2022;2:3. http://dx.doi.org/10.1186/s43593-021-00010-y.

[9] Shahriar MS, Pati GS, Tripathi R, Gopal V, Messall M, Salit K. Ultrahigh enhancement in absolute and relative rotation sensing using fast and slow light. Phys Rev A 2007;75:053807. http://dx.doi.org/10.1103/PhysRevA.75.053807.

[10] Shi J, Li M, Tang H, et al. Hybrid optical parametrically-oscillating emitter at 1930 nm for volumetric photoacoustic imaging of water content. eLight 2022;119:e2119705119. http://dx.doi.org/10.1186/s43593-022-00014-2.

[11] Duan LM, Lukin MD, Cirac JI, Zoller P. Long-distance quantum communication with atomic ensembles and linear optics. Nature 2001;414:413. http://dx.doi.org/10.1038/35106500.

[12] Zhao K, Xu X, Ren W, et al. Two-photon MINFLUX with doubled localization precision. eLight 2022;2:5. http://dx.doi.org/10.1186/s43593-021-00011-x.

[13] Chiao RY, Boyce J. Superluminality, parelectricity, and earnshaw's theorem in media with inverted populations. Phys Rev Lett 1994;73:3383. http://dx.doi.org/10.1103/PHYSREVLETT.73.3383.

[14] Gao L, Ma Y. Enhanced group velocity in composite media of particles with non-spherical shape or shape distribution. J Phys A 2005;38:7765. http://dx.doi.org/10.1088/0305-4470/38/35/010.

[15] Carreno F, Calderon OG, Antón MA, Gonzalo I. Superluminal and slow light in lambda-type three-level atoms via squeezed vacuum and spontaneously generated coherence. Phys Rev A 2005;71:063805. http://dx.doi.org/10.1103/PHYSREVA.71.063805.

[16] Ullah S, Akbar J, Qureshi MT, Elaimi MA, El-Kader MFHAbd, Usman M, Bacha BA. Laguerre fields strength and beam waist-dependent superluminal propagation of light pulse in atomic medium. Eur Phys J Plus 2022;137:963. http://dx.doi.org/10.1140/epjp/s13360-022-03074-y.

[17] Ma Y, Gao L. Subluminal and superluminal pulse propagation in inhomogeneous media of nonspherical particles. Phys Lett A 2006;355:413. http://dx.doi.org/10.1016/j.physleta.2006.02.039.

[18] Gao L. Decreased group velocity in compositionally graded films. Phys Rev E 2006;73:036602. http://dx.doi.org/10.1103/PhysRevE.73.036602.

[19] Arif SM, Bacha BA, Wahid U, Haneef M, Ullah A. Tunable subluminal to superluminal propagation via spatio-temporal solitons by application of laguerre fields intensities. Phys Lett A 2021;388:127041. http://dx.doi.org/10.1016/j.physleta.2020.127041.

[20] Simpson Tanner T, Pigeon Jeremy J, Ambat Manfred Virgil, Miller Kyle G, Ramsey Dillon, Weichman Kale, Froula Dustin H, Palastro John P. Spatiotemporal control of two-color terahertz generation. Phys Rev Res 2024;1(6):013041. http://dx.doi.org/10.1103/PhysRevResearch.6.013041.

[21] Sahrai M, Tajalli H, Kapale KT, Zubairy MS. Tunable phase control for subluminal to superluminal light propagation. Phys Rev A 2004;70:023813. http://dx.doi.org/10.1103/PHYSREVA.70.023813.

[22] Sahrai M, Etemadpour R, Mahmoudi M. Dispersive and absorptive properties of a lambda-type atomic system with two fold lower-levels. Eur Phys J D 2010;59:463. http://dx.doi.org/10.1140/EPJD/E2010-00172-X.

[23] Xiao F, Guo H, Li L, Liu C, Chen X. Enhanced effects of subluminal and superluminal propagation. Phys Lett A 2004;327:15. http://dx.doi.org/10.1016/j.physleta.2004.04.032.

[24] Yang Q, Seo JT, Tabibi B, Wang H. Slow light and superluminality in Kerr media without a pump. Phys Rev Lett 2005;95:063902. http://dx.doi.org/10.1103/PhysRevLett.95.063902.

[25] Wang S, Zhang H, Jiang J, Jiang L, Wu J. Tunable superluminal and subluminal reflected group delay in an air-weyl semimetal film-weyl semimetal substrate layered system. IEEE J Quantum Electron 2022;58:7000406. http://dx.doi.org/10.1109/JQE.2022.3181273.

[26] Dikopoltsev A, Sharabi Y, Lyubarov M, Lumer Y, Tsesses S, Lustig E, Segev M. Light emission by free electrons in photonic time-crystals. Proc Natl Acad Sci 2022;119:e2119705119. http://dx.doi.org/10.1073/pnas.2119705119.

[27] Wei XG, Wu JH, Wang HH, Li A, Kang ZH, Jiang Y, Gao JY. First-principles experimental observation of coherent hole-burnings in atomic rubidium vapor. Phys Rev A 2006;74:063820. http://dx.doi.org/10.1103/PhysRevA.74.063820.

[28] Tiaz Gul, Qureshi Haleema Sadia, Ghafoor Fazal. Controlled multiple spectral hole burning via a tripod-type atomic medium. New J Phys 2012;26:013047. http://dx.doi.org/10.1088/1367-2630/ad1eba.

[29] De Vries H, Wiersma DA. Homogeneous broadening of optical transitions in organic mixed crystals. Phys Rev Lett 1976;36:91, https://link.aps.org/doi/10.1103/PhysRevLett.36.91.

[30] Müller A, Richter W, Kador L. Persistent spectral hole-burning in the few-molecule limit: terrylene in p-terphenyl. Chem Phys Lett 1998;285:92. http://dx.doi.org/10.1016/S0009-2614(98)00007-4.

[31] Chanelière T, Bonarota M, Damon V, Lauro R, Ruggiero J, Lorgeré I, Le Gouët JL. Light storage protocols in tm: YAG. J Lumin 2010;130:1572. http://dx.doi.org/10.1016/j.jlumin.2009.12.025.

[32] Colice M, Schlottau F, Wagner KH. Broadband radio-frequency spectrum analysis in spectral-hole-burning media. Appl Opt 2006;45:6393. http://dx.doi.org/10.1364/ao.45.006393.

[33] Nilsson M, Rippe L, Kroll S, Klieber R, Suter D. Hole-burning techniques for isolation and study of individual hyperfine transitions in inhomogeneously broadened solids demonstrated in Pr^{+3}: Y_2SiO_5. Phys Rev B 2004;70:214116. http://dx.doi.org/10.1103/PhysRevB.70.214116.

[34] Li Y, Hemmer P, Kim C, Zhang H, Wang LV. Detection of ultrasound-modulated diffuse photons using spectral hole-burning. Opt Express 2008;16:14862. http://dx.doi.org/10.1364/oe.16.014862.

[35] Harris TL, Sun Y, Babbitt WR, Cone RL, Ritcey JA, Equall RW. Spatial-spectral holographic correlator at 1536 nm using 30-symbol quadriphase-and binary-phase-shift keyed codes. Opt Lett 2000;25:85. http://dx.doi.org/10.1364/ol.25.000085.

[36] Dong P, Gao JY. Appearance and disappearance of hole-burning behind an electromagnetically induced transparency window. Phys Lett A 2000;265:52. http://dx.doi.org/10.1016/S0375-9601(99)00863-4.

[37] Xiao ZH, Wu JH, Zhang HF, Gao JY. Comparison of coherent induced hole-burning between lambda, inverted lambda and ladder systems. Phys Lett A 2003;310:363. http://dx.doi.org/10.1016/S0375-9601(03)00462-6.

[38] Vadia S, Scherzer J, Watanabe K, Taniguchi T, Högele A. Magneto-optical chirality in a coherently coupled exciton–plasmon system. Nano Lett 2023;23:614. http://dx.doi.org/10.1021/acs.nanolett.2c04246.

[39] Khan Q, Bacha BA, Ahmad I, Khan M, Akgul A, EI Din SM, Khesro A. Manipulation of sensitivity of the surface plasmon polariton waves at the interface of high magneto-optical medium and silver metal using angular interrogation. Results Phys 2023;52:106844. http://dx.doi.org/10.1016/j.rinp.2023.106844.

[40] Bacha BA, Ahmad I, Ullah A, Ali H. Superluminal propagation in a polychromatically driven gain assisted four-level N-type atomic system. Phys Scr 2013;88:045402. http://dx.doi.org/10.1088/0031-8949/88/04/045402.

[41] Khan A, Mahmoud EE, Ahmad I, El Din SM, Bacha BA, Akgül A. Topological localized region of goos-hänchen shifts in reflection and transmission. Results Phys 2023;51:106738. http://dx.doi.org/10.1016/j.rinp.2023.106738.

[42] Ahmad R, Ali H, Ahmad I, Boutabba N. Spontaneously generated coherence in a four-level atomic system under induced chirality: Quantum control of the casimir force. Results Phys 2023;46:106314. http://dx.doi.org/10.1016/j.rinp.2023.106314.

[43] Wahid U, Khan A, Amin B, Ullah A. Surface plasmon hole-burning at the interface of cesium and gold by Kerr nonlinearity. Optik 2020;202:163651. http://dx.doi.org/10.1016/j.ijleo.2019.163651.

[44] Wu JH, Wei XG, Wang DF, Chen Y, Gao JY. Coherent hole-burning phenomenon in a Doppler broadened three-level type atomic system. J Opt B 2003;6:54. http://dx.doi.org/10.1088/1464-4266/6/1/009.

[45] Idrees M, Kalsoom H, Bacha BA, Ullah A, Wang LG. Continuum and undefine hole-burning regions via pulse propagation in a four-level Doppler broadened atomic system. Eur Phys J Plus 2020;135:698. http://dx.doi.org/10.1140/epjp/s13360-020-00705-0.